Journal of
Mechanics of
Materials and Structures

AN ENDOSCOPIC GRASPER WITH CORRUGATED PLATE-SHAPED TACTILE SENSORS

Mohammad Ameen Qasaimeh, Mohammadreza Ramezanifard and Javad Dargahi

Volume 4, № 5 May 2009

JOURNAL OF MECHANICS OF MATERIALS AND STRUCTURES
Vol. 4, No. 5, 2009

AN ENDOSCOPIC GRASPER WITH CORRUGATED PLATE-SHAPED TACTILE SENSORS

MOHAMMAD AMEEN QASAIMEH, MOHAMMADREZA RAMEZANIFARD AND JAVAD DARGAHI

One of the major weaknesses in current endoscopic surgery is the lack of tactile feedback. This paper reports on the design, finite element modeling, and experimental testing of a corrugated tactile sensor. The sensor, a miniaturized and modified form of our previously developed tactile sensor, consists of a 75 μm plate-shaped silicon layer and a 25 μm polyvinylidene fluoride (PVDF) film, patterned on both sides using photolithographic techniques to form three independent sensing elements. The sensor is 15 mm long, 7.5 mm wide, and approximately 3 mm thick, which could make it versatile enough for integration with current endoscopic and medical robotics manipulators. The silicon layer is micromachined in such a way that a U-channel is formed. When a force is applied on the tactile sensor, output voltages from the patterned PVDF-sensing elements are combined to obtain tactile information. Results show that the sensor exhibits high sensitivity and can measure small dynamic loads, comparable to a human pulse, as well as large grasping forces. In addition to measuring the magnitude and position of the applied load, the sensor can determine the modulus of elasticity of the grasped object.

1. Introduction

Over a decade ago, surgical procedures called minimally invasive surgery (MIS) were introduced. Though initially limited to specific kinds of operations, MIS has now become a standard and widely used surgical procedure, replacing most of the traditional open-surgery procedures [Tendick et al. 1998]. MIS has substantial benefits over traditional open surgeries, which require large incisions to allow the surgeon access to perform procedures at the operation site [Carrozza et al. 2003].

Tactile sensing is defined as the continuous sensing of variable contacting forces, such as the sensing ability of the human finger. One of the most exciting and rapidly emerging areas where tactile sensing is making a significant impact is in robotic surgery, primarily because soft tissue can only be properly recognized by evaluating its softness, viscosity, and elasticity properties [Rebello 2004]. In the decision-making process during surgery, one of the most highly evaluated procedures is palpation of tissues [Howe et al. 1995]. This is an essential step for any surgical process because palpation of the grasped tissue gives some ideas about its properties.

To perform MIS more effectively, the surgeon should be able to feel the tissue and sense the pressure of blood vessels and ducts during the surgical procedure [Howe et al. 1995; Rebello 2004]. This ability is imperative during manipulation tasks such as grasping internal organs, gentle load transfer during lifting, and suturing and removing tissues [Melzer et al. 1994]. Tactile sensors recommended for use during MIS procedures should be small, highly sensitive, have low manufacturing and integration costs, and should preferably be disposable [Carrozza et al. 2003; Rebello 2004; Qasaimeh et al. 2007]. Combining

Keywords: tactile sensor, endoscopic grasper, minimally invasive surgery, microfabricated sensor.

all of these features in MIS is one of the leading aspects of research with regard to the integration of microfabrication and microelectromechanical system (MEMS) technology in the field of tactile sensing and MIS. MEMS have both electrical and mechanical parts. The sensor, or actuator, fabricated using this technology, is micromachined to be relatively small in the macro world and includes microfabrications of both electrical and mechanical components on one common substrate. MEMS technology can be applied to the tactile-sensing field to produce tiny micro tactile sensors. These improved microfabricated tactile sensors have made great strides recently in the field of MIS, and many more promising improvements are in progress. Miniaturization of sensors improves dexterity and increases the sensing elements per unit area. These sensors can be mass produced, resulting in low unit costs.

Endoscopic and laparoscopic tools are widely used in MIS operations. Endoscope graspers should have teeth that are able to grasp slippery and soft tissues usually associated with endoscope operations [Rebello 2004]. A currently available commercial endoscopic tool for laboratory use is shown in Figure 1 (Snowden–Pencer Graspers SP90-3104 type).

Few publications exist that deal with tactile sensor design, especially for use in MIS. Some currently fabricated devices are able to find the force and compliance of sensed tissues but failed when it came to detecting embedded lumps, and were limited to a force range in the milligrams [Dargahi et al. 2000; 2005]. Finite element methods were applied in parallel development works [Tanimoto et al. 1998; Najarian et al. 2006], but none of the proposed designs had the ability to measure the position of the applied forces besides finding grasping forces. Narayanan et al. [2006] presented a tactile sensor for MIS operations, but the sensor is active only on the teeth regions; the other regions are inactive and unable to sense the properties of the contacting object. One of our developed sensors was presented in [Qasaimeh et al. 2007]. It was able to locate the applied force magnitude, pressure distributions on the organ, and embedded lumps; however, primary results indicate that the design is somewhat deficient in finding and detecting low-magnitude loads similar to the pulse in a blood vessel.

Based on our previous work [Qasaimeh et al. 2008a; 2008b; 2009], this paper presents a modified and miniaturized tactile sensor (15 mm long and 7.5 mm wide) which could be incorporated on the tip of MIS tools (such as an endoscopic tool or robotic manipulators). The presented sensor is able to measure the magnitude and position of grasping forces and is therefore could be potentially able to estimate any embedded lump or abnormality inside a grasped organ. In addition, the proposed sensor is able to detect low mechanical forces and hence can potentially detect the pulse in a blood vessel. Also, this sensor can estimate the softness of the object with which it comes into contact.

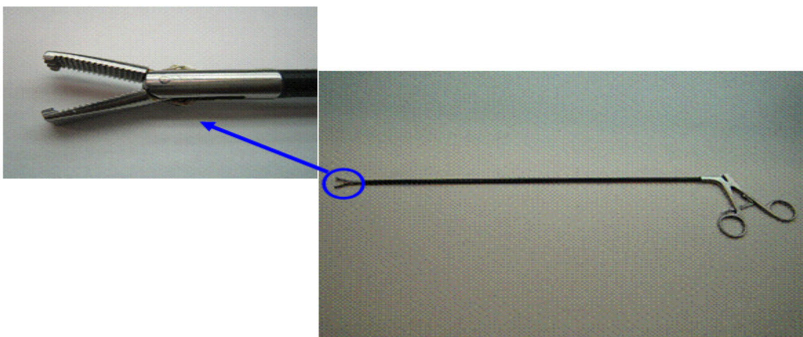

Figure 1. Commercial endoscopic graspers used for endoscopic surgeries (Snowden-Pencer SP90-3104).

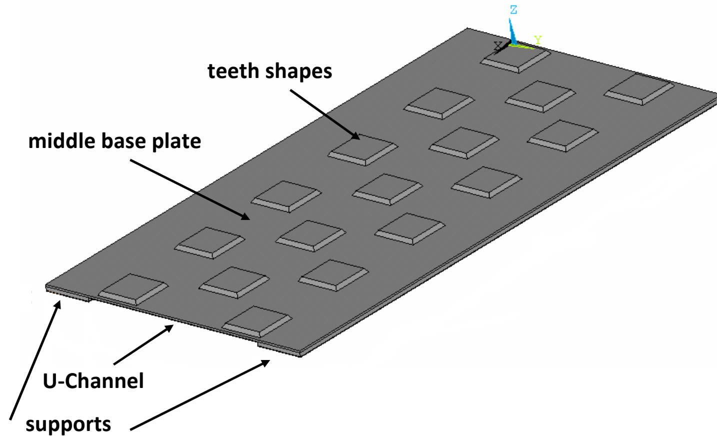

Figure 2. The silicon layer (first layer of the sensor assembly), comprising the teeth shape, the middle base plate, the U-channel, and the two supports.

2. Design and structure of the sensor

The proposed sensor is assembled using three layers. The first layer is micromachined from a silicon wafer. The second layer is the sensing element microfabricated by patterning a polyvinylidene fluoride (PVDF) film. Finally, the entire structure is supported by and attached to a substrate (third layer) of cage-shaped Plexiglas. The first layer is microfabricated to form the required teeth shapes of height 200 μm on the top of a deformable base plate of thickness 75 μm. The base plate stands on two supports, 200 μm in height, to form a U-shaped channel. All of these features are microfabricated in one step out of a single 475 μm silicon layer. The designed teeth on the top are necessary for the purpose of grasping. The microfabricated silicon layer design is shown in Figure 2, and a top view showing the teeth arrangements and dimensions is shown in Figure 3. The middle base plate is designed to give a deformation under grasping action, and the supports hold the base plate to provide a suitable gap which is necessary for the plate deflection. The second layer within the sensor is microfabricated from PVDF film to create sensing elements — specifically, from metalized and poled piezoelectric PVDF film, 25 μm thick [Qasaimeh et al. 2008a]. The third layer, or substrate, is machined out of Plexiglas to support the

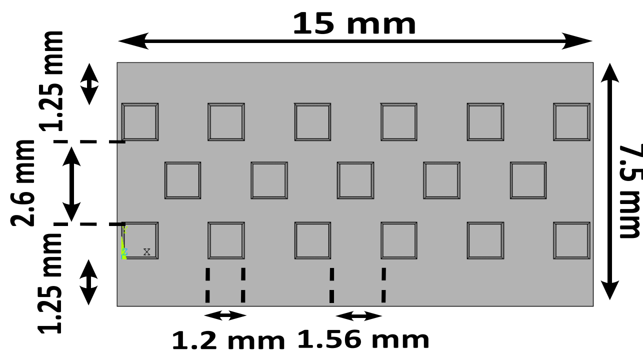

Figure 3. Top view of the sensor showing the teeth arrangement and dimensions. (The thickness is 3 mm.)

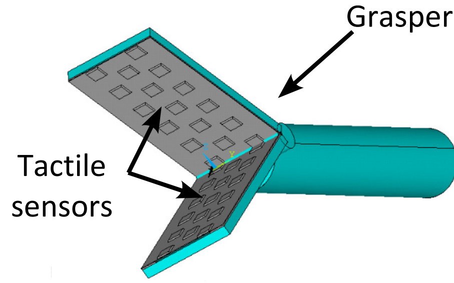

Figure 4. The proposed sensor after assembly and integration with an endoscopic MIS tool. A single sensor may be integrated with one jaw, or each jaw may be provided with its own sensor, allowing the combined signal to offer additional tactile information such as the depth of embedded lumps.

first two layers and hold them in place during tissue manipulation and operations such as handling, lifting and twisting. Plexiglas surrounds the first two layers on three sides (see Figures 10 and 11 on page 921) to protect the sensor assembly against shear forces associated with tissue manipulation. The integration between sensor and endoscopic grasper is schematically indicated in Figure 4.

The microfabricated prototype is 15 mm long and 7.5 mm wide. These dimensions are compatible with available commercial laparoscopic tools and could be easily integrated with them.

The silicon layer of the sensor base plate has a thickness of 75 μm. This thickness was chosen to optimize the loading range of the grasping forces as well as to be sensitive to the small mechanical forces which are equivalent to the pulse in a blood vessel. Moreover, after a study of various tooth-like shapes, an irregular teeth arrangement was chosen (as shown in Figures 3 and 4). The orientations of the attached PVDF were investigated and the drawn direction (d_{31}) of the PVDF-sensing elements was chosen to be parallel with the sensor width (Y-direction) [Qasaimeh et al. 2008b]. This proposed sensor is the second generation of our previously invented sensor and is based on our continuing work [Qasaimeh et al. 2008b; 2009]. The design of the sensing element has been modified to eliminate any cross-talk between adjacent elements, and the supporting layer was customized to protect the sensor assembly under shear stresses (during surgical manipulations) and eliminate the contribution of these stresses to the output signal. The size was also reduced so the sensor can fit with current endoscopic tools and medical robotic manipulators.

3. Principle of the sensor

There are two sensing layers in different locations. The first is the sensing layer at the supports, which is sandwiched between the silicon supports and the Plexiglas supporting layer. The second is the middle sensing layer which is glued to the back of the base plate. The sensing layer at the supports has two functions: it determines the total grasping force magnitude, and it locates any concentric load application. The middle sensing layer determines the grasped tissue softness and detects low magnitude forces.

While grasping internal organs, a compression force is transferred to the PVDF layers at the supports via the silicon layer. These forces will actuate the PVDF layers to work on its thickness mode, resulting in an output voltage on the electrodes. For greater compression loads, the PVDF layer will be compressed more, resulting in a higher magnitude of voltage. Because the silicon layer has two supports, we can

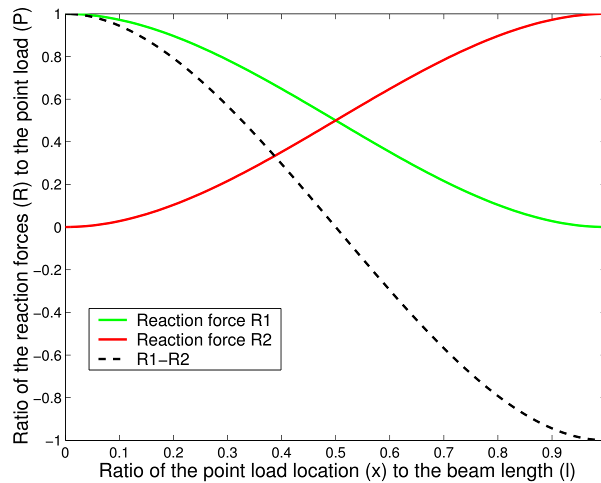

Figure 5. Reaction magnitudes as a function of the point load location. By comparing both quantities, the exact position of the applied point load can be estimated.

predict the applied load carried by these two supports using simple principles of mechanics. Depending on the pressure distributions and the concentric load location, the load will either be carried equally on both supports, or one of the supports will carry more than the other. For simplicity, a fixed-fixed simple beam with applied point load is considered. A point load P is applied at a distance x on the beam of length L. Two reactions, R_1 and R_2, and two moments, M_1 and M_2, appear at the fixed points of the beam. The magnitudes of both R_1 and R_2 are a function of x, and the summation of both is equal to the load magnitude P. Because the system is in static equilibrium, by equating to zero the sum of forces and the sum of moments, we obtain

$$R_1 = \frac{P(\ell^3 - 3\ell x^2 + 2x^3)}{\ell^3}, \qquad R_2 = \frac{P(3\ell x^2 - 2x^3)}{\ell^3}.$$

By plotting both equations versus the point load location, the relation between each reaction magnitude and the point load location is shown clearly (see Figure 5). By comparing both curves (R_1 and R_2), the exact position of the applied point load can be estimated.

The voltage generated at each sensing element beneath its support will depend on position with a shape similar to the one in Figure 5. The amplitude of the variation has the functional form

$$V = F\frac{d}{A \times C},$$

where F is the magnitude of the reaction forces, d is the piezoelectric coefficient of the sensing element (PVDF) in compression mode, A is the surface area of the sensing element, and C is the capacitance of the sensing element.

The middle sensing layer is a PVDF layer working on its extensional mode. Deflection of the base silicon plate will cause the PVDF layer to stretch and supply an output voltage. This sensing layer is responsible for determining tissue softness and for finding and responding to any low magnitude loading comparable to the pulse in a blood vessel. The silicon layer deflection is related to the softness of the contacting tissue. In the case of grasping a soft tissue, the silicon will yield to a large deflection (because

the tissue itself does not resist the action of the distributed load and bend easily), in proportion to the large stretching of the PVDF layer, and produce a high voltage. On the other hand, in the case of grasping a hard tissue, the silicon layer will be only slightly deflected (because the tissue itself will resist the bending action due to its rigidity) with correspondingly less stretching of the PVDF giving rise to only a small voltage.

4. Sensor modeling

A complete physical model of the proposed sensor was modeled and analyzed using ANSYS 12 (see Figure 6 for a top view of the mesh). This model is used to determine the deformation of the sensor and the output voltage at the PVDF-sensing elements for different loading conditions. Silicon and Plexiglas layers were modeled using the SOLID45 element, which possesses plasticity, creep, swelling, stress stiffening, large deflection, and large strain capabilities for 3D modeling. The PVDF-sensing elements were modeled using the SOLID227 element.

The linearized constitutive equations solved by the software are $\{\sigma\}_{6\times1} = [C]_{6\times6}\{\epsilon\}_{6\times1}$ and $D_{6\times1} = [e]^T_{6\times6}\{\epsilon\}_{6\times1}$, where σ is the stress vector, ϵ the strain vector, C the elasticity matrix, and D the electric flux density vector. The piezoelectric matrix can be defined either in the $[e]$ form (piezoelectric stress matrix) or in the $[d]$ form (piezoelectric strain matrix), the two being related by $[e] = [C][d]$.

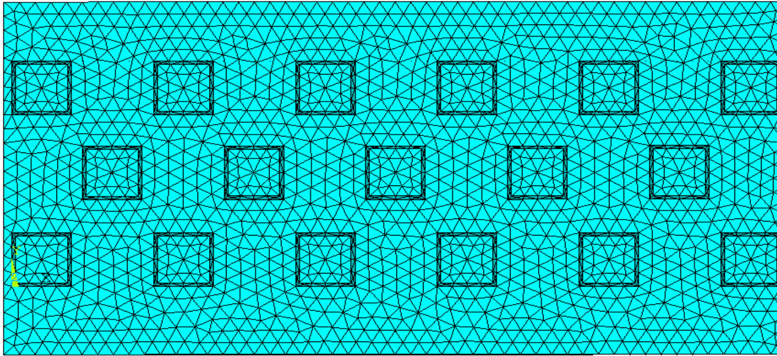

Figure 6. Top view of the meshed finite element model of the sensor.

5. Microfabrication and assembly

The silicon layer is microfabricated on both sides by employing anisotropic bulk etching using a tetramethylammonium hydroxide (TMAH) bath. The sensing elements are prepared by selectively etching each aluminum electrode covering the PVDF film on both sides. Each layer is prepared separately until the sensor is assembled.

Silicon microfabrications. The wafer is cleaned using deionized (DI) water and a nitrogen gun. It is then wet-oxidized in an oxidization furnace at 1100 °C for two hours to build a silicon oxide layer of almost 1.2 μm thickness. After oxidization, the silicon wafer is covered by a layer of Shipley S1813 positive photoresist (PR) by spin coating. It is then soft-baked on a hot plate at a temperature of 115 °C for about one minute. After preparing the dark field mask (which outlines the teeth shapes), the mask is

aligned to the flat edge of the wafer (100), using alignment marks, to have the {111} silicon planes on the side walls of the silicon teeth. This is followed by exposure to ultraviolet light for fifteen seconds. The PR is then developed, using an appropriate PR developer, and subsequently the sample is hard-baked on a hot plate at a temperature of 115 °C for one minute. After the careful alignments under the EVG mask aligner, the same procedure is repeated on the other surface of the silicon sample, using the second dark field mask which represents the supports. The next step is the wet-etching of the silicon oxide to form a hard mask for silicon bulk-etching. Oxide-etching begins by dipping the sample inside a buffered oxide etchant (HF) for a few minutes until the oxide-etching on the PR-free regions is complete. The remaining oxides act as the hard mask during the bulk silicon-etching process. The last step of the silicon layer microfabrication is the silicon bulk-etching inside a 25% TMAH bath. The sample is kept inside this bath for eleven hours to form teeth and supports with the desired heights and shapes. Finally, the remaining PR and silicon oxide is removed and the silicon sample is rinsed with DI water for a few minutes and dried using a nitrogen gun. The silicon microfabrication steps are shown in Figure 7.

PVDF fabrications. A sample of aluminum metalized PVDF film is prepared and cut with a rectangular shape and suitable dimensions. Care is taken that the drawn direction (d_{31}) of the PVDF strip is parallel with the width of the sample. The sample has dimensions $18 \times 8\,\text{mm}^2$, which is slightly wider and longer than the silicon sample to provide the necessary margins during assembly. The PVDF-sensing elements at both the middle and supports are microfabricated on single PVDF film. Therefore, both sides of the film are patterned to fabricate the PVDF-sensing elements at the middle and at the supports, and to ensure that all are electrically isolated from each other, thus eliminating cross-talk between elements.

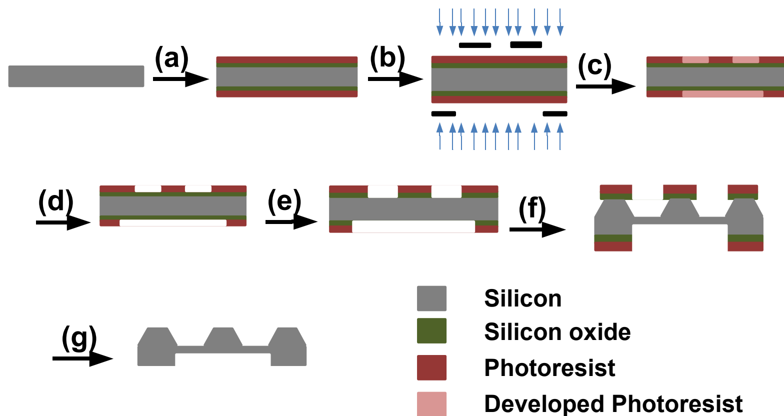

Figure 7. The silicon layer bulk etching process: (a) the silicon layer is thermally oxidized and photoresist is deposited on both surfaces; (b) the sample is soft-baked and then exposed to UV through different masks for each side; (c) the sample is hard-baked and then developed; (d) the developed photoresist is etched out; (e) unprotected silicon oxide is etched out; (f) unprotected silicon is etched out; (g) the remaining photoresist is removed, and then the silicon oxide is removed completely, resulting in the final microfabricated silicon layer.

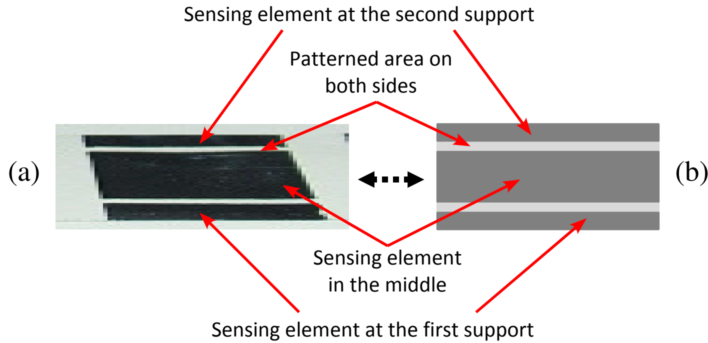

Figure 8. PVDF film and sensing elements: (a) the microfabricated PVDF sensing elements by patterning the PVDF film, and (b) designed PVDF sensing elements distribution on the PVDF film.

The three sensing elements are microfabricated using MEMS technology including the photolithography steps. The process starts with the PR deposition, and then the sample is soft-baked. After preparing the mask, the sample is exposed to UV light and the PR is hard-baked after developing. The same steps are then repeated for the other side of the sample after the care alignments under the EVG mask aligner. The aluminum cover is patterned using aluminum commercial etchant and then the remaining PR is removed. The patterned PVDF film, which includes the sensing elements, is shown in Figure 8. Finally, working under stereomicroscope, each aluminum electrode at each PVDF-sensing element is connected to a copper electrode (which, in turn, is welded to a copper wire connected to the conditioning circuit to provide the sensor's output) using conductive silver epoxy (see Figure 11 on the next page).

Layer assembly. First, the PVDF-sensing elements are glued to the microfabricated silicon layer. A nonconductive epoxy is distributed uniformly on the back of the middle silicon plate and on the bottom of both silicon supports as well. Afterwards, the PVDF sensing elements are aligned under a stereomicroscope to ensure their proper location. After that, as shown in Figure 9, compression blocks are applied for 24 hours to compress the sensing elements to the silicon layer to ensure secure and uniform adhesion. Finally, the Plexiglas layer is integrated into the structure using the same procedure; see Figure 10. The final assembled prototype sensor is shown in Figure 11.

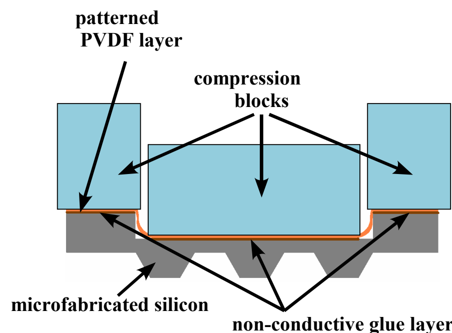

Figure 9. Assembly of the silicon and PVDF microfabricated sensor layers using nonconductive epoxy, with the application of compression blocks for 24 hours.

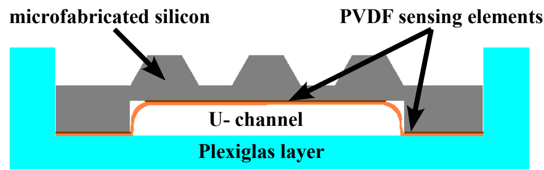

Figure 10. Final assembly of the sensor: the first two layers are fixed inside the Plexiglas cage with non-conductive epoxy, and compression is applied for 24 hours.

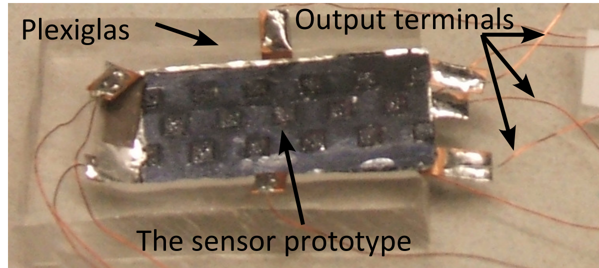

Figure 11. Photograph of the microfabricated prototype sensor.

6. Finite elements and experimental results

We now report and compare the simulation and experimental results. The experimental setup is shown in Figure 12. The sensor is fixed on an XYZ micropositioning stage and positioned under a cylindrical probe, which is driven by a vibration unit (Ling dynamic model V203) and used to apply a sinusoidal force of frequency 10 Hz, unless stated otherwise. The vibration unit is activated by a signal generator (Agilent 33220A).

The magnitude of the applied force is determined by a force transducer (KISTLER, Type 9712B50) inserted between the probe and the vibration unit. The force transducer output is connected to an amplifier which, in turn, is connected to a computer via the data acquisition card to monitor the applied load.

In the same way, the PVDF sensing elements are connected by wires to the charge amplifiers, which, in turn, are connected to a computer via the data acquisition card to measure output signals using the LabVIEW program.

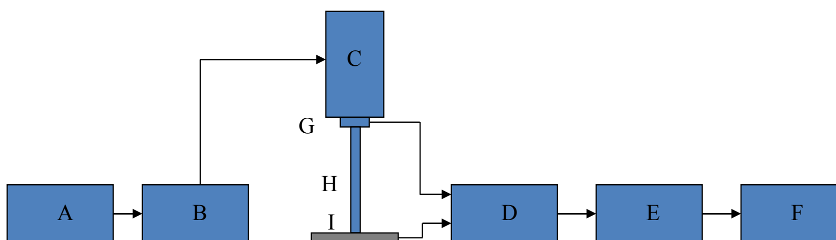

Figure 12. Experimental setup diagram: (A) signal generator, (B) power amplifier, (C) vibrator, (D) charge and voltage amplifiers, (E) A/D converter, (F) computer, (G) force transducer, (H) probe, and (I) the proposed sensor under test.

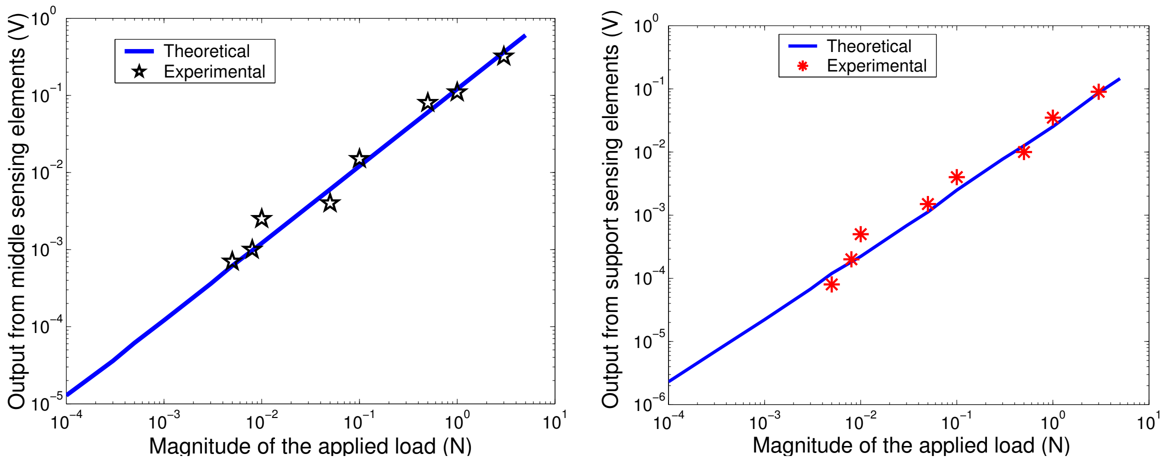

Figure 13. Left: calibration curve of the middle PVDF-sensing element. Right: calibration curve of each sensing element at the supports. For both curves, the experimental applied point loads ranged from 1 mN to 3 N and were always applied at the center of the sensor.

First, a point load is applied with a sharp head probe on the center point at the top of the sensor. This kind of loading is carried out in order to find a correlation between the output voltages in the PVDF-sensing elements with respect to the applied load magnitudes. Using this result, we obtained calibration curves for the sensor prototype, from which we can determine the grasping forces actually applied during surgery. The magnitudes of the forces applied ranged from 1 mN to 3 N. The output voltages with respect to the applied load magnitude at the PVDF-sensing elements are shown in Figure 13.

To detect the precise location of the applied point load, as when locating embedded lumps during surgery, a point load of 50 mN magnitude is applied on the silicon layer at different points. The point load was applied along the center line (which divides the length into two equal halves) of the silicon at different points in the Y-direction (crosswise). Output voltages from the middle PVDF-sensing element versus the 50 mN point load location are shown in Figure 14. To detect load location lengthwise, an array of sensing elements can be deployed along the sensor's length, as shown in [Qasaimeh et al. 2008b].

The output voltages versus the 50 mN point load location from the PVDF-sensing element at the first support (V_{S1}) and at the second support (V_{S2}) are shown in Figure 15. It can be seen from this figure that when a load is applied exactly onto the first support, the corresponding sensing element generates the maximum potential while the sensing element at the opposite support shows no output. Therefore, when the point of application moves away (along the Y-direction), the output voltage of the first support sensing element (V_{S1}) decreases and that of the second support (V_{S2}) increases. It is interesting to note that the difference between the output voltages of the pair of sensing elements at the supports (V_{S1} and V_{S2}) is linear with respect to the location of the applied concentric load. As a result, the location of applied load in the Y-direction can be calculated using this linear relationship.

Because the middle plate of silicon is thin (75 μm), it is therefore deformable under any action of forces. While contacting various tissues and objects, the plate will be deflected for small values if the tissue itself is hard. The reason for this is that hard tissue will resist bending under the load action. On

the other hand, where soft tissue is contacted, the plate will be deflected for larger values because soft tissue cannot resist bending as much as hard tissue can. When the plate deflects, the glued middle PVDF-sensing element at the back will be stretched and a voltage will be created. A larger deflection of the plate means that the PVDF layer will stretch even more, creating a correspondingly larger amount of voltage. Several simulations and experiments were carried out while considering different contacting objects with different moduli of elasticity. With a distributed load of 5 N applied to the top of a contacting object, theoretical and experimental results show that softer tissues cause a larger amount of created voltage, and harder contacting tissues cause a smaller amount of created voltage, as shown by the blue curve and red dots on Figure 16. In contrast, the output signals from the support sensing elements did not significantly

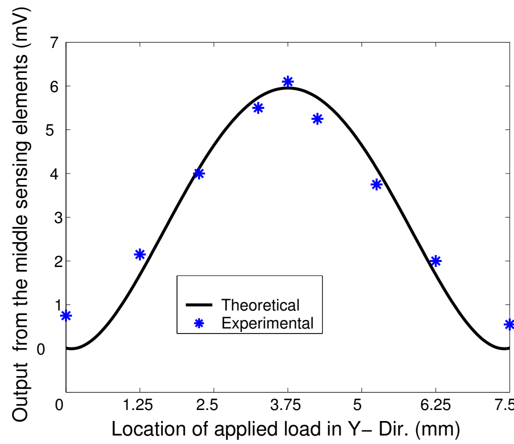

Figure 14. Output voltages from the middle sensing element versus the Y-location of the 50 mN point load. The maximum signal occurs when the force is applied exactly at the center of the sensor.

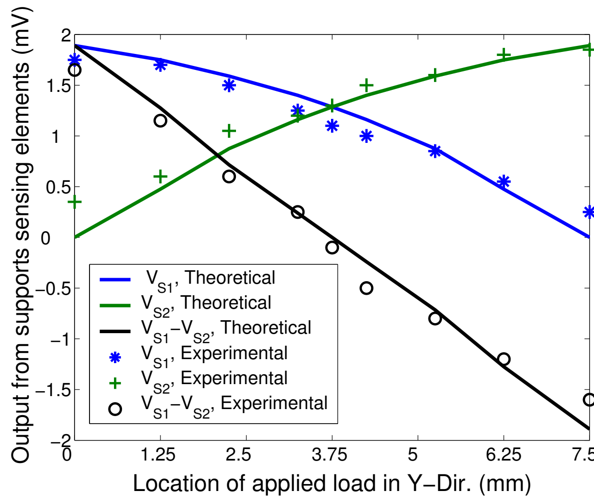

Figure 15. Output voltages from the first support sensing element (V_{S1}) and the second support sensing element (V_{S2}) versus the Y-location of the applied 50 mN point load.

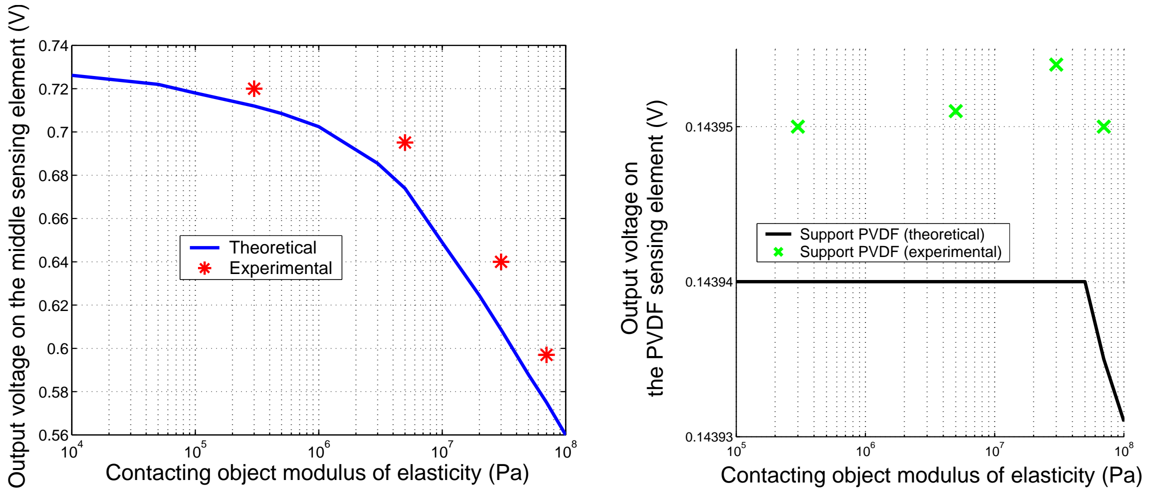

Figure 16. Theoretical and experimental values of the generated voltage on the sensing elements versus different modulus of elasticity of the contacting tissue, under application of a 5 N distributed uniform load. Left: middle sensing element. Right: support sensing element.

change with respect to the different contacting objects, as shown by the black curve and green dots in the same figure.

To test sensor response to an input comparable to the pulse of a blood vessel, a sinusoidal point load of 10 mN maximum amplitude and approximately 2 Hz frequency was applied at the middle of the sensor. The maximum response from the middle PVDF sensing element was found to be 2.2 mV, and the one from the support sensing elements, 0.3 mV. The output signals can be seen in Figure 17. In

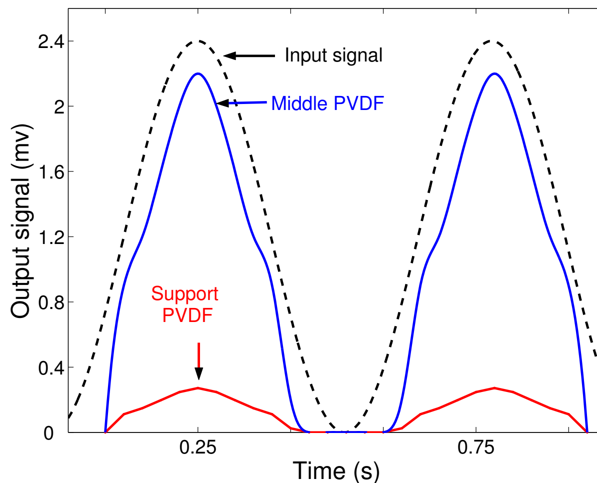

Figure 17. Experimental values of generated voltage on the support and middle sensing elements when a sinusoidal point load of amplitude 10 mN and frequency 2 Hz was applied on the middle of the sensor.

several experiments, we found that it is hard to see on the oscilloscope any response — especially from the support sensing elements — when the applied sinusoidal load is less than 1 mN (data not shown). As seen in the previous figure, the middle PVDF sensing element is more sensitive than the support sensing elements and can detect small dynamic loads comparable to the pulse of a blood vessel.

7. Discussion and conclusion

As shown in Figure 13, linear relations exist between the output voltages from PVDF-sensing elements and the magnitude of the applied loads. The voltage appearing in the middle of the PVDF-sensing element is the most sensitive and can detect low-magnitude applied loads comparable to a blood vessel pulse, as shown in Figure 17.

The summation of the two output voltages at the supports-sensing elements shows the total applied forces on the grasped object. As shown in Figures 14 and 15, the precise location of any point load is detectable by comparing the output voltage values of the PVDF-sensing elements. The detection of any point load indicates the capability of the sensor to detect the presence of an embedded lump inside the grasped tissue. As shown in Figure 16, the softness of the contacting object can be estimated using this novel plate design.

Differences between the theoretical and experimental results are due to many factors, one example of which is the electrical noise associated with the experimental setup. Another factor is the type of applied load. In theory, the applied load is a point force, but in experiments it is a sharp probe covering a small area. In addition, the contacting objects (tissues) used in the experiments are not ideal elastic objects; the known modulus of elasticity for each is not accurate and can even vary with different load applications. Also, the applied load in the simulations is static, but a low frequency dynamic sinusoidal load is applied in the experiments (peak-to-peak results were considered).

In conclusion, the potential sensor performance in relation to detecting grasping forces, embedded lumps, contacting tissues softness, and blood vessel pulse has been demonstrated. The sensor could be integrated with the commercial endoscopic tool for safer surgical procedures. Also, since it is micromachined, it could potentially be mass-produced with low unit cost, and be disposable.

However, improvements may need to be made before moving to the next stage of clinical test and use. One enhancement might be the use of an interface between the present sensor and graphical software, to display the contacting forces and tissue softness (as is being developed currently in our lab), or by integrating the sensor with a haptic interface to feel the contacting forces instead of monitoring them on a computer display. From the microfabrication point of view, direct deposition of PVDF on silicon chips as an alternative to gluing could make the sensor more precise. This might also help eliminate wiring to the PVDF sensing elements, leading to higher precision. Finally, proper packaging and protection is required for more effective functioning of the sensor.

References

[Carrozza et al. 2003] M. C. Carrozza, P. Dario, and L. P. S. Jay, "Micromechatronics in surgery", *Trans. Inst. Meas. Control* **25**:4 (2003), 309–327.

[Dargahi et al. 2000] J. Dargahi, M. Parameswaran, and S. M. Payandeh, "A micromachined piezoelectric tactile sensor for an endoscopic grasper: theory, fabrication and experiments", *IEEE/ASME J. Microelectromech. Sys.* **9**:3 (2000), 329–335.

[Dargahi et al. 2005] J. Dargahi, S. Najarian, and K. Najarian, "Development and three-dimensional modelling of a biological-tissue grasper tool equipped with a tactile sensor", *Can. J. Elect. Comput. Eng.* **30**:4 (2005), 225–230.

[Howe et al. 1995] R. D. Howe, W. J. Peine, D. A. Kontarinis, and J. S. Son, "Remote palpation technology", *IEEE Eng. Med. Biol. Mag.* **14**:3 (1995), 318–323.

[Melzer et al. 1994] A. Melzer, G. Buess, and A. Cuschieri, "Instrumentation and allied technology for endoscopic surgery", pp. 1–69 in *Operative manual of endoscopic surgery*, vol. 2, edited by A. Cuschieri et al., Springer, New York, 1994.

[Najarian et al. 2006] S. Najarian, J. Dargahi, and X. Z. Zheng, "A novel method in measuring the stiffness of sensed objects with applications for biomedical robotic systems", *Int. J. Med. Robot.* **2**:1 (2006), 84–90.

[Narayanan et al. 2006] N. B. Narayanan, A. Bonakdar, J. Dargahi, M. Packirisamy, and R. Bhat, "Design and analysis of a micromachined piezoelectric sensor for measuring the viscoelastic properties of tissues in minimally invasive surgery", *Smart Mater. Struct.* **15**:6 (2006), 1684–1690.

[Qasaimeh et al. 2007] M. A. Qasaimeh, J. Dargahi, M. Kahrizi, and M. Packirisamy, "Design and analysis of tactile optical sensor for endovascular surgery", pp. 67960J in *Photonics North 2007* (Ottawa, 2007), edited by J. C. Armitage, Proceedings of SPIE **6796**, SPIE, Bellingham, WA, 2007.

[Qasaimeh et al. 2008a] M. A. Qasaimeh, J. Dargahi, M. Kahrizi, and S. Najarian, "Characterization of a multifunctional tactile sensor for use in endoscopic surgeries", in *Tenth Pan American Congress of Applied Mechanics* (PACAM X) (Cancún, 2008), edited by T. L. Attard, 2008. To appear.

[Qasaimeh et al. 2008b] M. A. Qasaimeh, S. Sokhanvar, J. Dargahi, and M. Kahrizi, "A micro-tactile sensor for *in situ* tissue characterization in minimally invasive surgery", *Biomed. Microdevices* **10**:6 (2008), 823–837.

[Qasaimeh et al. 2009] M. A. Qasaimeh, S. Sokhanvar, J. Dargahi, and M. Kahrizi, "PVDF-based microfabricated tactile sensor for minimally invasive surgery", *IEEE/ASME J. Microelectromech. Sys.* **18**:1 (2009), 195–207.

[Rebello 2004] K. J. Rebello, "Applications of MEMS in surgery", *Proc. IEEE* **92**:1 (2004), 43–55.

[Tanimoto et al. 1998] M. Tanimoto, F. Arai, T. Fukuda, H. Iwata, K. Itoigawa, Y. Gotoh, M. Hashimoto, and M. Negoro, "Micro force sensor for intravascular neurosurgery and in vivo experiment", pp. 504–509 in *11th Annual International Workshop on Micro Electro Mechanical Systems* (*MEMS 98*) (Heidelberg, 1998), IEEE, New York, 1998.

[Tendick et al. 1998] F. Tendick, S. S. Sastry, R. S. Fearing, and M. Cohn, "Applications of micromechatronics in minimally invasive surgery", *IEEE/ASME Trans. Mechatron.* **3**:1 (1998), 34–42.

Received 12 May 2008. Revised 18 Apr 2009. Accepted 17 May 2009.

MOHAMMAD AMEEN QASAIMEH: mohammad.qasaimeh@mail.mcgill.ca
Biomedical Engineering Department, McGill University, 740 Dr. Penfield Avenue, Montreal, QC H3A 1A4, Canada

MOHAMMADREZA RAMEZANIFARD: m_ramez@encs.concordia.ca
Department of Mechanical and Industrial Engineering, Concordia University, 1455 De Maisonneuve Blvd. W, Montreal, QC H3G 1M8, Canada

JAVAD DARGAHI: dargahi@encs.concordia.ca
Department of Mechanical and Industrial Engineering, Concordia University, 1455 De Maisonneuve Blvd. W, Montreal, QC H3G 1M8, Canada